Iron–Sulfur Dimers with Benzimidazolate–Thiolate, –Phenolate or Bis(benzimidazolate) Terminal Chelating Ligands. Models for Rieske-type Proteins

Peter Beardwood and John F. Gibson*
Department of Chemistry, Imperial College of Science, Technology and Medicine, London SW7 2AY, UK

Complexes $[Fe_2S_2L_2]^{2-}$ **1–5** having terminal co-ordination by the ligands L^1–L^5 have been prepared and studied by a range of physical techniques as models for the Rieske-type proteins [H_2L^1 = 2-(2-mercaptophenyl)benzimidazole; H_2L^2 = 2-(2-hydroxyphenyl)benzimidazole; H_2L^3 = 2-(2-hydroxyphenyl)methylbenzimidazole; H_2L^4 = 2,2-bis(benzimidazol-2-yl)propane; H_2L^5 = 4,4-bis(benzimidazol-2-yl)heptane]. A preparation is described for $[NEt_4]_3[Fe_2S_2L^4_2]$ **6**, the first $[2Fe–2S]^+$ reduced complex to be isolated. The complexes have been characterised by UV/VIS, ^1H NMR and Mössbauer spectroscopies. Lack of heterogeneity in the ^1H NMR spectrum of the iron(II)–iron(III) complex **6** reveals valence averaging. On the Mössbauer time-scale the complex becomes valence-trapped as the temperature is lowered. The first reduction processes for **1–4** occur at potentials in the range −0.82 to −1.13 V. The positive shift produced by benzimidazolate co-ordination compared to thiolate is comparable to that for the Rieske-type proteins relative to tetracysteinyl ferredoxins. Benzimidazolate co-ordination is also found considerably to stabilise the trianionic chemical reduction products. These display frozen-solution ESR spectra with a range of lineshapes, analysis of which, taken together with previous data for $[2Fe–2S]^+$ complexes, indicates the ordering SS > NS > NN > OS > NO ≈ OO in ligand type as correlated with the magnitude of the lowest two *g* values. The Rieske-type proteins have *g* values which fit best with the last two ligand types of this series, suggesting a requirement for oxygen co-ordination.

Complexes $[Fe_2S_2(SR)_4]^{2-/3-}$ (R = alkyl) are well established analogues of the tetracysteinyl co-ordinated $[2Fe–2S]^{2+/+}$ centres in ferredoxin proteins, displaying many coincident physical and chemical properties.[1,2] In comparison a second differentiated group of [2Fe–2S] proteins have notably anomalous spectroscopic and redox properties which demonstrate a departure from tetrathiolate co-ordination.[3–5] Proteins of this type are widely observed in bacteria, plants and mammals, and may be given the term Rieske-type proteins, after the oldest known example identified in the mitochondrial bc_1 complex by Rieske *et al.*[6]

Whether the [2Fe–2S] co-ordination is homogeneous in type for the Rieske class of proteins, and the exact nature, number and geometry of the ligands involved, has yet to be fully resolved. Current evidence indicates a likely unsymmetrical co-ordination of the [2Fe–2S], with two non-sulfur ligands, probably both histidine nitrogens, at the iron which becomes Fe^{II} on reduction, and two cysteinyl sulfur ligands at the other iron.[7–12]

A recent study of site-directed mutagenesis in the *Saccharomyces cerevisiae* Rieske iron–sulfur protein at the six fully conserved putative cysteine or histidine [2Fe–2S] ligands found that all were essential for cluster incorporation and enzymatic activity.[13] However, according to Gatti *et al.*[14] inactive proteins devoid of [2Fe–2S] also result for this yeast strain from mutations of aspartic, glycine, serine or proline non-ligand amino acids in the carboxyl-terminal cluster-binding region.

As with the ferredoxins, so too with the Rieske-type [2Fe–2S] proteins it is important to have available synthetic model complexes to facilitate a detailed understanding of the physical and chemical properties of the metal centres. Here we describe $[Fe_2S_2L_2]^{2-}$ complexes **1–5**, having bidentate benzimidazolate–thiolate, benzimidazolate–phenolate or bis(benzimidazolate) terminal chelating ligands (L = L^1–L^5). The synthesis and properties of the first isolable reduced $[2Fe–2S]^+$ complex, $[Fe_2S_2L^4_2]^{3-}$ **6** are also reported. Some of the results have been described briefly in a previous communication.[15]

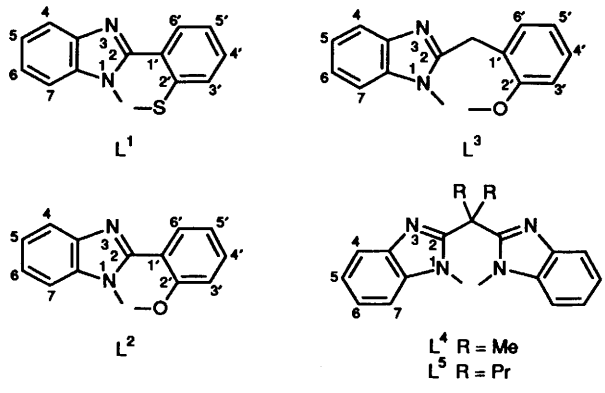

Experimental

General.—Dimethylformamide (dmf, Aldrich HPLC grade) was dried over molecular sieves. Acetonitrile was distilled from CaH_2. Diethyl ether was dried over sodium wire. The salt $[NBu^n_4]ClO_4$, prepared from $[NBu^n_4]Br$ and perchloric acid, was recrystallised three times from ethyl acetate and dried at 120 °C.

All preparations and manipulations of the [2Fe–2S] complexes were carried out under argon or dinitrogen on a vacuum/inert gas manifold using septum seals. Solution and suspension transfers were accomplished using stainless-steel or poly(tetrafluoroethylene) (ptfe) tubes inserted through the seals.

Ligand Synthesis.—Ligands H_2L^1, H_2L^2 and H_2L^3 were prepared by condensation of 1,2-diaminobenzene with the corresponding carboxylic acid in polyphosphoric acid.[16,17] While this synthetic method is also applicable to H_2L^4 with R = H in place of Me (using malonic acid),[18] for R = Me the

elevated temperatures required led to decarboxylation and yielded 2-iso-propylbenzimidazole. The dialkyl derivatives L^4 and L^5 could, however, be prepared from the corresponding dinitriles as described below.

2,2-*Bis(benzimidazol-2-yl)propane* (H_2L^4). Dimethylmalononitrile[19] (4.7 g, 50 mmol) and finely powdered 1,2-diaminobenzene dihydrochloride (18.1 g, 100 mmol) were heated at 185 °C under N_2 for 3 h with occasional stirring. The temperature was then raised to 200–210 °C for 4 h. After cooling, the resulting intensely blue solid was dissolved from the reaction flask using 1 mol dm^{-3} aqueous HCl (200 cm^3). The solution was decolorised by boiling with charcoal, filtered and after cooling brought to pH 8 by adding ammonia solution. The resulting cream precipitate was filtered off and repeatedly washed with water by dispersion and refiltering. Finally the solid was washed with EtOH (200 cm^3) and after drying over P_2O_5 under vacuum 9.7 g (70%) of product was obtained (Found: C, 73.6; H, 5.8; N, 20.3. Calc. for $C_{17}H_{16}N_4$: C, 73.90; H, 5.85; N, 20.25%). ^{13}C NMR [D_2O–HCl, reference dimethyl sulfoxide (dmso) δ 40.5]: δ 27.0 (Me), 40.1 (central C), 115.8 and 128.8 (C^{4-7} of C_6 ring), 132.6 (C_6 ring adjacent to N), and 153.2 (C^2 of benzimidazole).

4,4-*Bis(benzimidazol-2-yl)heptane* (H_2L^5). The dinitrile $Pr^n_2C(CN)_2$[19] (7.5 g, 50 mmol) and finely powdered 1,2-diaminobenzene dihydrochloride (19.9 g, 110 mmol) were mixed and heated to 230–240 °C for 9 h under N_2 with occasional stirring. After cooling the dark green solid was extracted by vigorous boiling first with four 60 cm^3 aliquots of 0.5 mol dm^{-3} HCl then with three 300 cm^3 aliquots of 0.3 mol dm^{-3} HCl. The extracts were decolorised by boiling with charcoal, filtered and after cooling neutralised with aqueous NH_3. The resulting cream coloured solid was filtered off and repeatedly washed with water by dispersing and refiltering to give a total crude yield of 13.7 g (83%) after thorough drying. Recrystallisation was accomplished by dissolving the product in boiling EtOH (*ca.* 900 cm^3), treating with charcoal, filtering and boiling down to around 300 cm^3. After cooling 9.4 g (57%) of fine white needle crystals were produced. Further product could be obtained from the EtOH solution. Melting point 310.5–311 °C (Found: C, 75.95; H, 7.35; N, 16.8. Calc. for $C_{21}H_{24}N_4$: C, 75.85; H, 7.30; N, 16.85%). ^1H NMR [$(CD_3)_2SO$]: δ 0.85 (10, CH_2Me), 2.5 (4, CH_2), 7.2 and 7.55 (8, H^{4-7}) and 12.4 (2, NH).

[2Fe–2S] *Complex Synthesis.*—The $[NEt_4]^+$ or $[AsPh_4]^+$ salts of $[Fe_2S_2L_2]^{2-}$ were prepared from $[Fe_2S_2Cl_4]^{2-}$ by ligand exchange with Na_2L (L = L^1–L^5). A representative preparation is detailed below.

$[NEt_4]_2[Fe_2S_2L^2_2]$. 2-(2-Hydroxyphenyl)benzimidazole (840 mg, 4 mmol) was dissolved and deprotonated using NaOMe (8 mmol) (generated *in situ* from NaH) in MeOH (4 cm^3) under Ar. The solvent was evaporated at reduced pressure with gentle heating and the resulting white solid dried under vacuum for 2 h and then taken up in deoxygenated dmf (30 cm^3). This solution was added over 30 min to a stirred solution of $[NEt_4]_2[Fe_2S_2Cl_4]$[20] (1.16 g, 2 mmol) in dmf (30 cm^3) under Ar. After stirring for 45 min the deep red solution was filtered, Et_2O (200 cm^3) added and the whole left at −25 °C for 15 h. The supernatant, which had then lost most of its colour, was withdrawn and the somewhat oily solid was washed with Et_2O and dried under vacuum. The product was extracted at 45 °C with three portions of MeCN totalling around 100 cm^3 and filtered through dried Celite filter medium leaving behind a dark amorphous solid. Diethyl ether was added to bring the solvent volume to around 300 cm^3 and the maroon microcrystalline product collected after 15 h of standing at ambient temperature. The recrystallisation was repeated in a similar manner except that occasionally it was found necessary to add a small amount of dmf in order to accomplish complete dissolution. The yield was 960 mg (56%).

The above method was also utilised in preparing the $[AsPh_4]^+$ salts of $[Fe_2S_2L_2]^{2-}$ for L = L^1 or L^2. For L^3 and L^5 and for L^1 with $[NEt_4]^+$ cation and L^4 with $[AsPh_4]^+$ cation, MeCN was replaced by dmf in the recrystallisation steps. For L^4 with $[NEt_4]^+$ as cation the somewhat different procedure described below was followed.

$[NEt_4]_2[Fe_2S_2L^4_2]$. 2,2-Bis(2-benzimidazolyl)propane (1.1 g, 4 mmol), was treated with NaOMe (8 mmol) in MeOH (5 cm^3) under Ar and after stirring for 15 min the solvent was removed under reduced pressure. The resulting white solid was dried for 2 h under vacuum, dissolved in dmf (60 cm^3) and added over 45 min to $[NEt_4]_2[Fe_2S_2Cl_4]$ (1.16 g, 2 mmol) in dmf (60 cm^3) at −10 °C with stirring under Ar. Stirring was continued for 3 h at room temperature and the red-brown precipitate collected by filtration on Celite. This solid was washed with dmf (50–100 cm^3) to remove a deep red contaminant with spectral absorption maxima at 555, 490 and 375 nm. Once the washings appeared pale and gave only the spectrum of the desired product (Fig. 2), the remaining solid was gradually dissolved in dmf (*ca.* 500 cm^3) at 40–45 °C and passed through the filter. Diethyl ether (500 cm^3) was added with stirring and the solution left for 15 h at room temperature. The red-brown product collected by filtration was washed well with Et_2O and dried under vacuum to yield 1.02 g (52%). The restricted solubility of complex **4** (*ca.* 2 mg per cm^3 in dmf) makes it difficult to obtain better than a microcrystalline form of the solid. However, **5**, which is around 100 times more soluble in dmf, can readily be induced to form a crystalline product.

This and the other diiron(III) solids can be handled briefly in air without detriment.

$[NEt_4]_3[Fe_2S_2L^4_2]$ **6**. Acenaphthylene (0.456 g, 3 mmol) in dmf (25 cm^3) under argon was treated with an amalgam of 1.5 g Na in 150 g Hg and stirred at the interface for 2 h. Meanwhile, $[NEt_4]_2[Fe_2S_2L^4_2]$ (0.49 g, 0.5 mmol) and $NEt_4Cl{\cdot}xH_2O$ (0.11 g) (dried over P_2O_5 under vacuum) were dissolved in deoxygenated dmf (280 cm^3) at *ca.* 40 °C and filtered through dried Celite. The solution was further deoxygenated by bubbling Ar through for 1 h. Then the sodium acenaphthylenide solution (4.8 cm^3, 1.15 equivalents) was added by syringe in aliquots (*ca.* 0.5 cm^3) over a period of 15 min, with vigorous stirring. The reduction was accompanied by a substantial loss of colour. An ESR sample taken at this point demonstrated quantitative reduction to the trianion. After 30 min more of stirring, deoxygenated Et_2O (700 cm^3), treated with the sodium acenaphthylenide solution (1 cm^3) to reduce any oxidant contaminants, was added slowly and caused the product to precipitate from solution as microcrystalline plates. Stirring was continued for 30 min and then the solid was allowed to settle. After 30 min the hazy supernatant was withdrawn and the product filtered off, washed with Et_2O and dried thoroughly under vacuum to yield 430 mg (77%). This solid was handled only in a glove-box.

Elemental Analysis.—The C, H and N analyses were performed by the Butterworth Laboratory, Imperial College Chemistry Department. Some of the compounds for which a satisfactory H and N analysis was obtained, and which by ^1H NMR spectroscopy were structurally identifiable and confirmed to be without significant impurities, frequently gave low and erratic carbon analyses. This is not without precedent for benzimidazole complexes. Elemental analyses for complexes **1**–**6** are: $[NEt_4]_2[Fe_2S_2L^1_2]$ (Found: C, 56.25; H, 6.35; N, 9.5. Calc. for $C_{42}H_{56}Fe_2N_6S_4$: C, 57.00; H, 6.40; N, 9.50); $[NEt_4]_2[Fe_2S_2L^2_2]$ (Found: C, 58.4; H, 6.75; N, 9.45. Calc. for $C_{42}H_{56}Fe_2N_6O_2S_2$: C, 59.15; H, 6.60; N, 9.85); $[AsPh_4]_2$-$[Fe_2S_2L^2_2]$ (Found: C, 65.65; H, 4.45; N, 4.05; S, 4.70. Calc. for $C_{74}H_{56}As_2Fe_2N_4O_2S_2$: C, 65.40; H, 4.15; N, 4.10; S, 4.70); $[AsPh_4]_2[Fe_2S_2L^3_2]$ (Found: C, 63.3; H, 4.45; N, 4.05. Calc. for $C_{76}H_{60}As_2Fe_2N_4O_2S_2$: C, 65.80; H, 4.35; N, 4.05); $[AsPh_4]_2[Fe_2S_2L^4_2]$ (Found: C, 65.65; H, 4.55; N, 7.3. Calc. for $C_{82}H_{68}As_2Fe_2N_8S_2$; C, 66.05; H, 4.60; N, 7.50); $[NEt_4]_2[Fe_2S_2L^4_2]$ (Found: C, 57.6; H, 6.65; N, 13.4. Calc. for $C_{50}H_{68}Fe_2N_{10}S_2$: C, 60.95; H, 6.95; N, 14.20); $[NEt_4]_2$-

$[Fe_2S_2L^5{}_2]$ (Found: C, 61.8; H, 7.9; N, 12.4. Calc. for $C_{58}H_{84}Fe_2N_{10}S_2$: C, 63.50; H, 7.70; N, 12.75); $[NEt_4]_3[Fe_2S_2L^4{}_2]$ (Found: C, 61.85; H, 7.95; N, 13.5. Calc. for $C_{58}H_{88}Fe_2N_{11}S_2$: C, 62.45; H, 7.95; N, 13.80%).

Reductions.—The iron–sulfur dimers were reduced as previously described[21] using *ca.* 1.1 equivalents of monosodium acenaphthylenide in dmf or *N*-methylpyrrolidinone, with subsequent rapid transfer of samples of the solutions to ESR tubes for immediate freezing in liquid nitrogen.

Physical Measurements.—Electronic absorption spectra were measured using 1 mm silica cells on a Perkin-Elmer 551 or a Philips PU8740 spectrophotometer, ^1H NMR spectra of the complexes in 99.9% $(CD_3)_2SO$ (Aldrich, dried over molecular sieves) at 25–30 °C using a JEOL FX90Q (90 MHz) or Bruker WM250 (250 MHz) spectrometer.

Mössbauer measurements were made on samples (*ca.* 100 mg) of powder in nylon containers (19 mm diameter) at 77 K in zero field using a *ca.* 10 mCi $^{57}Co/Rh$ source and Cryophysics MS103 instrumentation calibrated using iron metal at 298 K.

The ESR spectra of frozen solutions in silica tubes (5 mm diameter) at 77 K in a finger Dewar were measured on a Varian E12 instrument for which the frequency was calibrated using an Elliott Bros. WM 16 wavemeter and the field using a Varian NMR gaussmeter. The pure solvents normally crystallised on freezing to give an opaque sample unless $[NBu^n{}_4]ClO_4$ was added (usually 0.1 mol dm^{-3} for dmf, 0.2 mol dm^{-3} for *N*-methylpyrrolidinone), in which case they froze in a vitreous state. Yields of reduced species were measured by double integration of their ESR spectra in comparison to a 3 mmol dm^{-3} copper-ethylenediaminetetraacetate standard, which usually was measured in the same ESR tube. Simulations were made using the program EPRPOW originally written by White and Belford[22] and modified by one of the authors.[23]

A PAR 174A polarographic analyser and a Metrohm rapid dropping mercury electrode (r.d.m.e.) operating at six drops per second were used to perform electrochemical measurements on *ca.* 1–2 mmol dm^{-3} solutions of the complexes in dmf containing 0.1 mol dm^{-3} $[NBu^n{}_4]ClO_4$ supporting electrolyte. A platinum counter electrode was contained in a compartment separated from the bulk solution by a coarse frit. A saturated calomel or Ag–AgCl reference electrode contacted the solution *via* an aqueous KCl bridge with a fibre junction to a 0.1 mol dm^{-3} $[NBu^n{}_4]ClO_4$–dmf bridge terminating in a Vycor porous plug.

Results and Discussion

Synthesis and Chemical Properties.—The $[2Fe–2S]^{2+}$ complexes have been reported with a variety of terminal ligand types: bis(thiolate),[24] dihalide,[25] bis(selenophenolate),[26] S_5,[27] Se_5,[28] bis(phenolate),[29–31] bis(pyrrolate),[29] carboxylate–thiolate[32] and phenolate–thiolate.[29,33] The $[Fe_2S_2L_2]^{2-}$ complexes reported here introduce three additional co-ordination types: thiolate–benzimidazolate, phenolate–benzimidazolate and bis(benzimidazolate). Their formation from $[Fe_2S_2Cl_4]^{2-}$ by displacement of chloride with the deprotonated ligands L = L^1–L^5 in an aprotic solvent [reaction (1)] follows the

$$[Fe_2S_2Cl_4]^{2-} + 2Na_2L \longrightarrow [Fe_2S_2L_2]^{2-} + 4NaCl \quad (1)$$

procedure previously adopted[29–33] and represents a simple method of exploring the potential of new ligands to co-ordinate $[2Fe–2S]^{2+}$.

We have undertaken such investigative reactions without successfully isolating a $[Fe_2S_2L_2]^{2-}$ complex for a number of benzimidazole-derived ligands: 2,2′-bis(benzimidazolate), 4-carboxybenzimidazolate and 2-(2-mercaptoethyl)benzimidazolate led to intractable solids; 2-mercaptomethylbenzimidazolate and 2-(2-hydroxyphenyl)-1-methylbenzimidazole gave no identifiable $[2Fe–2S]^{2+}$ product: 2,2-bis(1-methylbenzimidazol-2-yl)propane did not react. With H_2L = 1,2-bis(benzimidazol-2-yl)ethane a $[Fe_2S_2L_2]^{2-}$ complex did result, but being difficult to purify was not fully characterised.

For H_2L = bis(benzimidazol-2-yl)methane (L_4 with R = H) only an impure pyrophoric paramagnetic solid could be isolated from reactions of the deprotonated ligand with $[Fe_2S_2Cl_4]^{2-}$. In solution this showed a strong ESR signal with *g* values of 2.013, 1.930 and 1.875 typical of a $[2Fe–2S]^{+}$ reduced centre. Only when the methylene protons were replaced by methyl (L^4) or propyl (L^5) groups were we able to isolate purely the desired bis(benzimidazolate) co-ordinated $[2Fe–2S]^{2+}$ complex. Similarly H_2L = bis(imidazolyl)methane led to a paramagnetic product with *g* values of 2.012, 1.924 and 1.853. The ability of this ligand to effect reduction of Fe^{III} on complexation has been reported recently.[34] With 2,2-bis(imidazolyl)propane the $[2Fe–2S]^{2+}$ bis(imidazole) complex could be prepared and recrystallised, but was not fully characterised.

The $[Fe_2S_2L_2]^{2-}$ complexes are soluble to varying degrees in dmf, *N*-methylpyrrolidinone or dmso and are stable in solution for prolonged periods. Although complexes **1**–**3** may possibly crystallise from solution with the ligands in a specific geometrical arrangement, when dissolved they are expected, very rapidly, to attain an equilibrium distribution between the isomers, due to the facile ligand exchange typical of these types of complexes.

On addition of a small excess of benzenethiol, complexes **2**–**4** are converted cleanly into $[Fe_2S_2(SPh)_4]^{2-}$, as monitored by optical spectrophotometry and ^1H NMR spectroscopy.

The reduction of complex **4** with sodium acenaphthylenide [reaction (2)] follows the method used to prepare $[Fe_4S_4(SR)_4]^{3-}$ complexes.[35] The compound $[NEt_4]_3[Fe_2S_2L^4{}_2]$ is the first example of a synthetic $[2Fe–2S]^{+}$ reduced cluster to be isolated in solid form.

$$[NEt_4]_2[Fe_2S_2L^4{}_2] + NEt_4Cl + NaC_{12}H_8 \longrightarrow [NEt_4]_3[Fe_2S_2L^4{}_2] + NaCl + C_{12}H_8 \quad (2)$$

Spectroscopic and Electrochemical Properties.—*Electronic spectra.* The electronic spectra for complexes **1**–**4** and for **6** in dmf are depicted in Figs. 1 and 2. Wavelengths and absorption coefficients for their main features are collected in Table 1. The spectra and data are presented chiefly for characterisation purposes, however certain observations concerning the likely origin of specific absorption bands may be noted.

For complexes **2** and **3** intense absorption maxima occur at 396 and 404 nm respectively and are attributable to (aryl)O→Fe charge transfer as observed for $[Fe_2S_2(OPh)_4]^{2-}$ at 404 nm and more generally in the range 390–420 nm for a variety of phenolate co-ordinated iron(III) complexes.[33] Of the $[2Fe–2S]^{2+}$ complexes, **1** has the most intense absorption at low energy from a broad band at *ca.* 580 nm, which is considered to arise from (aryl)S→Fe charge transfer. This transition gives rise to a deconvoluted band at *ca.* 553 nm for $[Fe_2S_2(SPh)_4]^{2-}$ for which the assignment has been corroborated by a matching resonance-Raman excitation profile for the symmetric stretching vibrational mode of the terminal ligands.[36] Both the shape and the intensity of the visible spectrum for **1** are very similar to those for the complex $[Fe_2S_2(O_2CC_6H_4S\text{-}2)_2]^{2-}$ which has spectral features at *ca.* 560 (ε 7.1 × 10^3) and 505 nm (7.9 × 10^3 dm^3 mol^{-1} cm^{-1}).[32]

The band in the region 510–525 nm common to complexes **1**–**4** may probably be assigned, at least in part, to charge transfer within the $[2Fe–2S]^{2+}$ centre.

The spectral profile of complex **5** is very similar to that for **4**. On one-electron reduction of these two complexes there is a dramatic loss of intensity in the visible absorption region. In Fig. 2 a comparison is made of the spectrum for the diiron(III) complex **4** and the $[2Fe–2S]^{+}$ reduction product **6**, for which the main feature in the visible region is a relatively weak

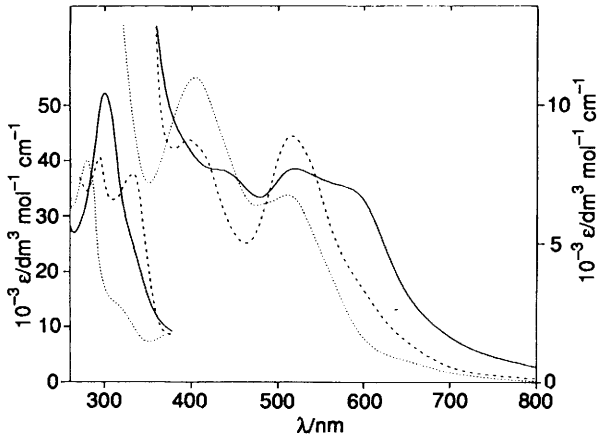

Fig. 1 Electronic absorption spectra for complexes **1** (——), **2** (– – – –) and **3** (· · · ·) in dmf

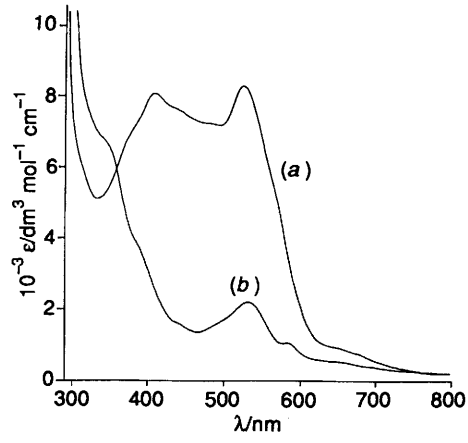

Fig. 2 Electronic absorption spectra for (*a*) $[Fe_2S_2L^4_2]^{2-}$ **4** and (*b*) $[Fe_2S_2L^4_2]^{3-}$ **6** in dmf

Table 1 Electronic absorption spectral parameters from dmf solutions

Compound*	λ/nm (ε/10^3 dm^3 mol^{-1} cm^{-1})
1	580 (sh, ap) (7.1), 517 (7.7), 435 (sh, ap) (7.5), 301 (52)
2	516 (8.9), 396 (8.7), 332 (37), 293 (41)
3	510 (6.7), 404 (11.0), 315 (sh, ap), 280 (40)
4	525 (8.3), 409 (8.1), 375 (sh, ap), 280 (49)
6	650 (sh, ap), 585 (1.0), 530 (2.1), 350 (sh, ap)

sh = shoulder, ap = approximate.
* Cations: **1**, $[NEt_4]^+$; **2**, $[AsPh_4]^+$; **3**, $[NEt_4]^+$ or $[AsPh_4]^+$; **4**, $[NEt_4]^+$ or $[AsPh_4]^+$; **6**, $[NEt_4]^+$.

absorption at 530 nm. Comparable peaks are observed on reduction in dmf solution for **1** at 555 nm and for **2** at 530 nm. For each of these reduced $[2Fe–2S]^+$ species reoxidation, by brief admission of air to the solution with mixing, results in 85–90% restoration of the spectrum for the diiron(III) complex.

^{1}H *NMR*. Chemical shifts of the ligand proton resonances of complexes **1**–**6** in $(CD_3)_2SO$ are listed in Table 2. In order to facilitate characterisation, details of the NMR spectra at both 90 and 250 MHz are reported for $[NEt_4]^+$ or $[AsPh_4]^+$ salts. These spectra show dipolar broadened isotropically contact-shifted resonances in the δ −1 to −13 region, typical of [2Fe–2S] complexes having aryl ligands.

For many of the resonances of complexes **1**–**3** a small splitting occurs which can be attributed to the geometric co-ordination isomerism expected in solution. These split peaks, most prominent at 250 MHz, are paired in Table 2 for purposes of assignment. For **2** the resonances from the two isomers are of approximately equal intensity, while for **3**, and still more pronouncedly for **1**, the downfield peak of each pair has the greater intensity, indicative of a thermodynamically favoured geometric arrangement in the isomeric equilibrium.

Intensities of the ligand proton resonances for the six complexes relative to those for their cations are consistent with the expected co-ordination of one ligand per iron.

Assignment of the NMR features, given in Table 2, can be made on the basis of the following observations. Since the paramagnetic relaxation time is proportional to the sixth power of the dipolar separation a pronounced broadening is anticipated for proton H^7 which is expected to be in close proximity to the Fe. This renders it beyond detection at 250 MHz in complexes **1**–**5**. Each of these complexes possesses resonances at *ca.* −5.3 to −5.5 and *ca.* −6.8 to −7.2 corresponding in intensity to one proton each per benzimidazole ring. The origin of these peaks can be established by comparing the spectrum of **2** with that for the corresponding compound having 5,6-dimethyl substituents on the benzimidazole ring. This shows peaks at δ −11.32, −11.10, −10.66 and −10.50 (3 ^{1}H per ligand) but no further resonances up to *ca.* −4. The resonance at δ *ca.* −7.0 for **4** and **5** is approximately twice as broad as those at δ *ca.* −5.5 or *ca.* −10.6 and is therefore attributable to the protons H^6, which are closer to the [2Fe–2S]$^{2+}$ centre than are H^5 or H^4.

Assignment of the remaining peaks for complexes **1**–**3** follows by analogy with previously reported thiolate and phenolate [2Fe–2S]$^{2+}$ complexes[31–33,37] which show a pattern of alternating paramagnetic shifts for the resonances of the ligand aromatic ring, positive for *ortho*- and *para*-protons and negative for *meta*-protons. Such a pattern can be attributed to dominant contact interactions involving ligand → Fe antiparallel spin transfer and spin delocalisation *via* ring π orbitals to afford positive spin density at *o*-C and *p*-C and negative density at *m*-C through spin correlation.[38,39] The resonances of $[Fe_2S_2(SPh)_4]^{2-}$ at δ −9.31 (*m*), −4.90 (*o*) and −3.38 (*p*) are comparable to those of the thiolate ring in **1**. However, the proton $H^{6'}$ in this complex has a resonance at δ *ca.* −10.9, more comparable to that of δ −10.3 found for $[Fe_2S_2(O_2CC_6H_4S\text{-}2)_2]^{2-}$ for the *m*-proton which is *ortho* to the carboxylate. A similar downfield shift is observed in **2** for $H^{6'}$ relative to $H^{4'}$, but is absent in **3** where the adjacent π-bonded substituent is one carbon removed.

The ^{1}H NMR spectrum for complex **6** represents the first available for a synthetic [2Fe–2S]$^+$ reduced complex. The three most prominent peaks are not greatly shifted from their positions in the spectrum of **4** and are assigned in the same way. As for **4** the peak assignable to H^6 at δ −6.37 is broader than those from the more remote H^5 and H^4. However, the individual resonance lineshapes are slightly narrower for **6** than their counterparts for **4**, indicative of the very high electronic spin relaxation rate at ambient temperature. Possibly as a consequence of this a relatively broad peak at δ *ca.* −6.8 is detectable in the 250 MHz spectrum, attributable to H^7. On brief admission of air the spectrum of **6** changes to that of **4**.

Integration relative to the cation resonances and the absence of other peaks out to δ −50 indicates that the four resonances assigned for complex **6** represent all the ligand ring protons. This lack of heterogeneity is the most significant observation from the ^{1}H NMR spectrum of **6** as it contrasts with the distinction between iron(II)–ligand and iron(III)–ligand resonances characteristic of charge-localised [2Fe–2S]$^+$ proteins.[40–42] Thus, no localisation of iron-(II) and -(III) is apparent for **6** in solution on the NMR time-scale.

^{57}Fe *Mössbauer*. Isomer shift (δ), quadrupole splitting (ΔE_Q) and linewidth (Γ, half-width) parameters from Lorentzian least-squares fitting of ^{57}Fe Mössbauer spectra for solid samples of complexes **1**–**4** at 77 K and zero magnetic field are reported in Table 3. The spectra consist of single sharp quadrupole doublets with linewidths not significantly larger than the

Table 2 Proton NMR data for complexes **1**–**6** in $(CD_3)_2SO$

Complex	δ at 90 MHz	δ at 250 MHz	^1H per ligand	Assignment
1	−11.15* (sh, ap)	−11.10*	} 2	$H^4 + H^{6'}$
	−10.91*	−10.94,* −10.85*		
	−9.81	−9.75*	1	$H^{4'}$
	−7.24, −6.92	−7.21,* −6.88*	1	H^6
	−5.37	−5.41,* −5.33*	1	H^5
	−4.45	−4.54,* −4.27*	1	$H^{3'}$
	−3.13*	−3.23,* −3.09*	1	$H^{5'}$
2	−11.4* (sh, ap)	−11.4 (sh)	} 3	$H^4 + H^{6'} + H^{4'}$
	−11.33, −11.04	−11.32, 11.04		
	−10.85, −10.66	−10.85, 10.65		
	−6.99	−7.00	1	H^6
	−5.35	−5.44, −5.31	1	H^5
	−3.31,* −2.92*	−3.36,* −2.99*	1	$H^{5'}$
3	−10.8* (sh, ap), −10.50*	−10.83, −10.50	3	$H^4 + H^{4'} + H^{6'}$
	−6.97	−6.80,* −6.98*	1	H^6
	−5.48	−5.50	1	H^5
	−1.98*	−2.08,* −1.93*	1	$H^{5'}$
	−8 (vbr, ap)	−8.5 (br, ap)		CH_2
4	−10.61	−10.58	2	H^4
	−7.06	−7.04	2	H^6
	−5.48	−5.48	2	H^5
	−3 (br, ap)	−3 (br, ap)		Me
5	−10.74	−10.73	2	H^4
	−6.98	−6.97	2	H^6
	−5.53	−5.53	2	H^5
		−1.75	4	α-CH_2
		−0.90	6	Me
6	−12.21, −12.16	−12.19	2	H^4
		−6.8 (br, ap)	2	H^7
	−6.37	−6.38	2	H^6
	−5.32	−5.33	2	H^5
		−3.21 (br)		Me

sh = shoulder, ap = approximate, br = broad. Assignments indicate the ring position as marked on the formulae.
* $[AsPh_4]^+$ cation, otherwise $[NEt_4]^+$.

instrumental linewidth, similar to those found for other $[2Fe–2S]^{2+}$ complexes. Thus, the Mössbauer spectra do not show evidence of the geometric isomerism demonstrated in solution by ^1H NMR spectroscopy. This is not unexpected in view of the anticipated insensitivity of the Mössbauer parameters to such variability in the terminal ligation. Comparisons drawn in Table 3 with a range of other $[2Fe–2S]^{2+}$ synthetic complexes show quite a small variation in isomer shift, making this parameter of limited utility in characterising terminal ligand types. However, it is possible to conclude that while phenolate co-ordination leads to an increased isomer shift compared with thiolate, heterocyclic nitrogen somewhat reduces the shift. This latter is consistent with a decreased iron(II) character and suggests that benzimidazolate is relatively less electron donating or covalent in bonding.

Mössbauer data for the $[2Fe–2S]^{2+}$ centre in the Rieske protein from *Thermus thermophilus* is given in Table 3. The iron sites are differentiated by unsymmetrical co-ordination such that one has $\delta = 0.24$ mm s^{-1} and is probably co-ordinated by two cysteinyl ligands, while the other has a pH-dependent isomer shift $\delta = 0.28$ (pH 10) or 0.32 mm s^{-1} (pH 7.8)[43] associated with non-cysteinyl ligands of uncertain type and structural geometry. The relative insensitivity of the isomer shifts of $[2Fe–2S]^{2+}$ complexes to changes in terminal ligation, coupled with the variability found amongst tetracysteinyl co-ordinated ferredoxins (δ = *ca.* 0.2–0.3 mm s^{-1}), precludes unequivocal application of this parameter in ligand diagnosis for the proteins. However, although none of the co-ordination types studied here (NS, NO, NN) appears ruled out by the isomer shift data, the (NO) ligated complexes **2** and **3** are observed most closely to match the values for the iron site which is considered to have non-cysteinyl co-ordination in the Rieske-type proteins.

Examination of the quadrupole splittings listed in Table 3 reveals a correlation between large ΔE_Q values and inflexible tight chelate co-ordination by the ligand. Lower values of ΔE_Q are associated with monodentate ligands or the more flexible chelates.

For the reduced $[2Fe–2S]^+$ centre in ferredoxins and Rieske-type proteins Mössbauer spectra reveal localised iron-(II) and -(III) sites.[4,44–49] Thus, zero-field spectra at high temperatures (above *ca.* 200 K) show two well resolved quadrupole doublets with parameters typical of a high-spin iron(III) and a high-spin iron(II) site. At low temperatures (*e.g.* 4.2 K), where the electron-spin relaxation rate has become slow relative to the nuclear precession frequencies, the Mössbauer spectra show splittings due to magnetic hyperfine interactions. For a range of external fields these spectra can be analysed as resulting from the negative and positive hyperfine fields of antiparallel spin-coupled iron-(II) and -(III) components. This valence-trapped analysis was also found appropriate for the Mössbauer spectra of $[Fe_2S_2\{(SCH_2)_2C_6H_4\text{-}o\}_2]^{3-}$.[21]

The zero-field Mössbauer spectrum of complex **6** at ambient temperature (295 K) approximates to an unsymmetrical quadrupole doublet ($\delta \approx 0.44$, $\Delta E_Q \approx 1.3$ mm s^{-1}). On cooling to *ca.* 77 K and lower a second doublet component ($\delta \approx 0.67$, $\Delta E_Q \approx 2.7$ mm s^{-1}) gradually increases in contribution to an extent of around 50%. The spectra are complicated at the lower temperatures as the electron-spin relaxation approaches the Mössbauer time-scale. Similar temperature-dependent spectral series are observed for dmf solutions of ^{57}Fe-enriched **6** and reduced **2**. The spectra can be interpreted as arising from a localised iron(II)–iron(III) mixed-valence core at low temperature which gradually undergoes thermal valence detrapping as the temperature is raised. At some point in the series of spectra the temperature-dependent rate of the interiron electron-

Table 3 ^{57}Fe Mössbauer parameters[a]

$[Fe_2S_2L_2]^{2-}$	Cation	δ[b]	ΔE_Q	Γ[c]	Ref.
1	$[AsPh_4]^+$	0.25	0.89	0.14	
2	$[NEt_4]^+$	0.27	1.24	0.15	
3	$[NEt_4]^+$	0.29	0.70	0.13	
4	$[NEt_4]^+$	0.25	0.90	0.12	
Ligand (L)					
$O_2CC_6H_4S$-2	$[AsPh_4]^+$	0.28	1.18	0.14	
$O_2CC_6H_4CH_2S$-2	$[AsPh_4]^+$	0.29	1.06	0.16	
$O_2CCH_2C_6H_4S$-2	$[AsPh_4]^+$	0.31	0.79	0.14	
$OC_6H_4CH_2S$-2	$[NEt_4]^+$	0.28	0.99	0.14	33[d]
2-$OC_6H_4C_6H_4S$-2	$[NEt_4]^+$	0.29	0.95	0.25	33[d]
2,2′-$(OC_6H_4)_2$	$[NEt_4]^+$	0.35	1.02		29
$(OPh)_2$	$[NEt_4]^+$	0.37	0.32	0.13	30
$(SPh)_2$	$[NEt_4]^+$	0.28	0.32	0.13	30
$(SCH_2)_2C_6H_4$-*o*	$[NEt_4]^+$	0.28	0.36	0.13	30
$\{N(CH)_3CH\}_2$	$[NEt_4]^+$	0.26	0.49		29
Protein					
Ferredoxin		0.2–0.3	0.6–0.8		21
Rieske pH 7.8, 4.2 K		0.24	0.52	0.13	4
(*Thermus*)		0.32	0.91	0.13	
Rieske pH 10, 4.2 K		0.24	0.44		43
(*Thermus*)		0.28	0.70		
Benzene dioxygenase		0.23	0.45		44
(*P. putida*)		0.33	1.03		

[a] In mm s^{-1} at 77 K, unless otherwise stated. Standard deviations on the computer-fitted parameters from this work are less than the quoted accuracy of ± 0.005 mm s^{-1}. [b] Relative to iron metal at ambient temperature. [c] Linewidth expressed as the half-width at half-height. [d] Linewidths given in ref. 33 are incorrectly described as full linewidths. In fact they are half-widths at half-height.

Table 4 Electrochemical half-wave reduction potentials in dmf[a]

	$E_{\frac{1}{2}}$ (r.d.m.e.)/V	
$[Fe_2S_2L_2]^{2-}$	2−/3−	3−/4−
1	−0.99	−1.87
2	−1.09	−1.97
3	−1.13	−1.95
4	−0.82	−1.81
Ligand (L)		
$(SPh)_2$	−1.14	−1.45
$(SCH_2)_2C_6H_4$-*o*	−1.51	−1.79
$(SEt)_2$	−1.44	−1.69
$(OR)_2$[b]	−1.35	−1.80
$O_2CC_6H_4S$-2	−1.02	−1.84
$OC_6H_4CH_2S$-2	−1.44	

[a] Rapid dropping-mercury electrode rate was *ca.* 6 drops s^{-1}. Potentials are relative to a saturated calomel electrode. [b] R = aryl. Average value.

transfer process approximates to the Mössbauer time-scale at around 10^7 s^{-1}. Thus, the observation of equivalent iron sites in the 300 K ^{1}H NMR spectra of **6** is consistent with their anticipated rapid electron exchange relative to the NMR time-scale.

Mössbauer spectra over a range of temperatures and magnetic fields show a complexity, due to the combined effects of the two varying dynamic processes of intervalence electron transfer and electron-spin relaxation, which necessitates careful and detailed analysis in order to determine accurate Mössbauer, nuclear and electronic parameters. A description of this work will be presented in a future publication.

Electrochemistry. Polarography (d.c.) of the complexes in dmf shows two reduction waves at a rapid dropping-mercury electrode with the half-wave potentials given in Table 4. Reduction potentials for related [2Fe–2S] complexes measured under the same conditions are also listed.

Potentials for the first reduction, assigned to $[2Fe–2S]^{2+/+}$, appear to be approximately additive in terms of the functional groups of the co-ordinating ligands. Thus, the average of these half-wave potentials for the tetra(benzimidazolate) **4** and for $[Fe_2S_2(SPh)_4]^{2-}$, at −0.98 V, is very close to the $E_{\frac{1}{2}}$ for **1** (−0.99 V). Similarly **2** and **3** have first reduction potentials at around the average of those for **4** and $[Fe_2S_2(OR)_4]^{2-}$ (R = aryl). On this basis it seems reasonable to attempt to circumvent the difficulties of direct electrochemical comparisons between Rieske proteins and model complexes due to differences in milieu and method of measurement by instead comparing shifts in potential relative to examples of [2Fe–2S] centres having similar co-ordination environments.

Amongst the model complexes listed in Table 4, $[Fe_2S_2(SEt)_4]^{2-}$ represents the best approximation to co-ordination by four cysteines, as found in $[2Fe–2S]^{2+}$ ferredoxins. Such proteins typically have midpoint redox potentials of around -0.35 ± 0.1 V (relative to the standard hydrogen electrode)[50] which are much lower than those characteristic of Rieske-type proteins, for example +0.14 V for the [2Fe–2S] protein from *T. thermophilus*[43] and −0.11 V for benzene dioxygenase from *Pseudomonas putida*.[51] The positive shifts for these Rieske-type proteins relative to ferredoxins give a range of around +250 to +500 mV which is comparable to the $E_{\frac{1}{2}}$ shifts of +350 mV for **2** and +620 mV for **4** relative to $[Fe_2S_2(SEt)_4]^{2-}$. Such comparisons are inadequate to the extent that the Rieske-type proteins most likely have the unsymmetrical co-ordination $(RS)_2FeS_2FeX(Y)$ (X and Y = imidazolate, imidazole, phenolate or carboxylate) rather than the symmetric ligation of **1**–**4**. However, if the additive effects of co-ordinated functional groups on reduction potential bear significantly on only the one half of the iron dimer which receives the electron, then the data from the model complexes do indicate that replacement of an alkanethiolate ligand by an anionic imidazolate donor is sufficient to cause a positive shift of the order found for some Rieske proteins. On the same basis imidazolate–phenolate co-ordination at one iron would predicate a similar shift. However, in the absence of other contributing factors, such as variant protein charge distribution, two imidazolates would be required to produce the large positive shifts found for some Rieske proteins.[52,53] Ligation by neutral imidazole would be expected to cause increased electrostatic stabilisation of the reduced form and consequent raising of the redox potential, due to a lowering of the formal charge on the cluster.[54]

The positive shifts in $E_{\frac{1}{2}}$ for complexes **1**–**4** relative to $[Fe_2S_2(SEt)_4]^{2-}$ indicate that benzimidazolate is less capable of transferring electron density to the $[2Fe–2S]^{2+}$ core than is thiolate. This is consistent with the Mössbauer isomer shift results.

While the potentials of the first reduction waves for complexes **1**–**4** represent the least negative extent of the range for synthetic $[2Fe–2S]^{2+/+}$ complexes, the corresponding second reduction waves, attributed to $[2Fe–2S]^{+/0}$, are amongst the most negative in potential. This large potential difference between first and second one-electron reduction processes, most notable for **4** at 0.99 V, may be a factor in the relative stability of the benzimidazolate co-ordinated $[Fe_2S_2L_2]^{3-}$ species, since it will lead to a far lower equilibrium concentration of the unstable diiron(II) complex resulting from the disproportionation reaction $2[2Fe–2S]^+ \rightleftharpoons [2Fe–2S]^{2+} + [2Fe–2S]^0$. For **6** the equilibrium constant for this reaction will be around 10^{12} times smaller than for the most stable tetrathiolate co-ordinated $[2Fe–2S]^+$ complex, $[Fe_2S_2\{(SCH_2)_2C_6H_4\text{-}o\}_2]^{3-}$, which has a half-life in dmf of <5 min. Of the reduced $[2Fe–2S]^+$ complexes not having benzimidazolate co-ordination $[Fe_2S_2(O_2CC_6H_4S\text{-}2)_2]^{3-}$ has considerably the largest separation in potential between oxidation and reduction processes and significantly is also by far the most stable, with a solution half-life of *ca.* 30 min.

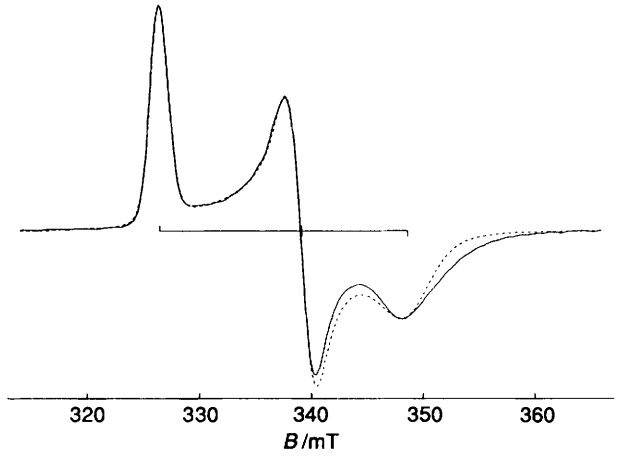

Fig. 3 The ESR spectrum for reduced complex **1** in dmf at 77 K (——) together with a simulation (– – – –) according to the parameters in Table 5. The markers at baseline level show the g values derived from the simulation. Concentration *ca.* 0.4 mmol dm^{-3}, microwave frequency 9.20 GHz, microwave power 8 mW, modulation amplitude 0.32 mT

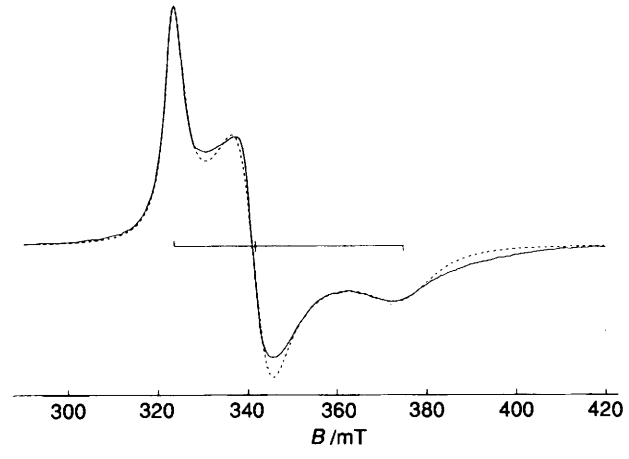

Fig. 4 The ESR spectrum for reduced complex **2** in dmf at 77 K (——) together with a simulation (– – – –) according to the parameters in Table 5. The markers at baseline level show the g values derived from the simulation. Concentration *ca.* 1.5 mmol dm^{-3}, microwave frequency 9.18 GHz, microwave power 12 mW, modulation amplitude 0.63 mT

Table 5 ESR parameters from simulations

	$[Fe_2S_2L_2]$ complex reduced			
	1	**2**	**4**	**5**
g_1	2.014	2.027	2.012	2.017
g_2	1.938	1.920	1.933	1.930
g_3	1.886	1.750	1.875	1.854
$g_2 - g_3$	0.052	0.170	0.058	0.076
g_{av}	1.946	1.899	1.940	1.934
Lorentzian half-width/mT				
1	0.2	2.5	1.7	1.4
2	0.6	2.2	2.2	2.1
3	1.6	7.5	4.5	3.7
Gaussian half-width/mT				
1	0.9	0.5		
2	1.0	2.9		
3	1.8	3.7		

Cyclic voltammetry of complexes **1**–**4** at glassy carbon or platinum electrodes gives well formed pairs of cathodic current

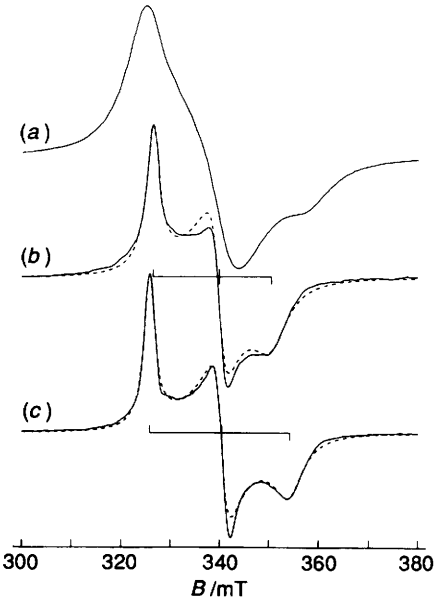

Fig. 5 The ESR spectra at 77 K for (*a*) solid $[NEt_4]_3[Fe_2S_2L^4_2]$, (*b*) reduced **4** in dmf containing 0.25 mol dm^{-3} $[NBu^n_4]ClO_4$ and (*c*) reduced **5** in dmf containing 0.1 mol dm^{-3} $[NBu^n_4]ClO_4$. The dashed lines are simulations using the parameters of Table 5 and the markers at baseline level show the g values employed. Concentration in (*b*) and (*c*) is *ca.* 0.3 mmol dm^{-3}; microwave frequency 9.20 GHz; microwave power (*a*) 0.2, (*b*) 20, (*c*) 12 mW; modulation amplitude (*a*) 0.2, (*b*) 0.63, (*c*) 0.4 mT

maxima and anodic current minima for the first reduction process, centred at potentials within 5 mV of those observed at the r.d.m.e. For **1** and **4** the cathodic and anodic peak currents are approximately equal using a 100 mV s^{-1} scan rate. The second reduction in these complexes is somewhat less reversible, but the anodic peak is well developed in each case and mid-peak potentials are within 5 mV of those given in Table 4. Complexes **2** and **3** show only a cathodic peak for their second reductions, the absence of any corresponding anodic current minimum being attributable to gross irreversibility of electron transfer in these cases. The first reduction cycle for **2** appears approximately reversible ($i_c/i_a \approx 1$) but is complicated by a small unresolved broad feature at around −1.0 V which is also seen in the d.c. polarogram. Other small impurity or decomposition-product features were seen at the following approximate potentials: **1**, −1.6; **2**, −0.55, −1.45; **3**, −0.5, −1.55 V.

ESR. Figs. 3–5 show ESR spectra for frozen dmf solutions of complexes **1**, **2**, **4** and **5** quantitatively reduced with sodium acenaphthylenide and for the solid **6**. Table 5 lists anisotropic g values and linewidths employed in calculating the simulated lineshapes overlaid on the solution spectra. For reduced **3** in frozen dmf a broad axial spectrum is observed[15] with g_1 = 2.031 and the baseline cross-over at g = 1.878. The broad hyper-Lorentzian lineshape of this spectrum does not allow accurate determination of g_2 and g_3 by simulation.

Similar principal g values to those of Table 5 are found for spectra obtained from *N*-methylpyrrolidinone or dmso frozen solutions. The linewidths, however, vary considerably with solvent and concentration. The spectrum of reduced **5** in Fig. 5(*c*) is better resolved than that for reduced **4** in Fig. 5(*b*), which in turn is rather better resolved than the lineshape previously reported for pure dmf.[15] This can be attributed in the first place to the enhanced solubility conferred by propyl ligand substituents compared to methyl substituents and secondly to the addition of $[NBu^n_4]ClO_4$ to the solvent which causes it to freeze as a glass. Both these factors mitigate the solute aggregation present when the solvent crystallises. On additional dilution of reduced **5** in dmf the g_1 line half-width drops further from 1.4 to *ca.* 1 mT.

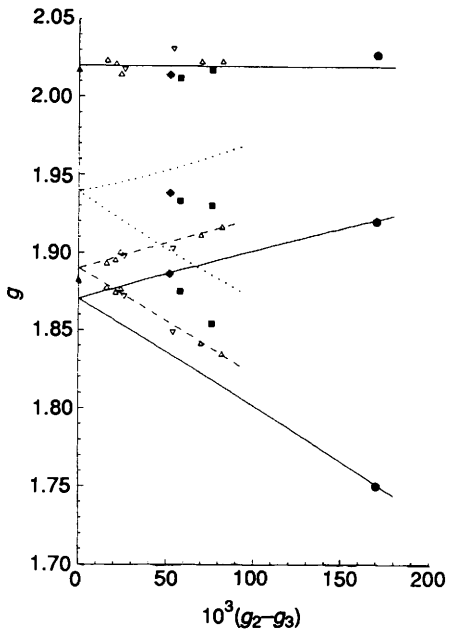

Fig. 6 A plot of principal g values against the splitting of the lowest two g values for $[Fe_2S_2L_2]^{3-}$. The lines were calculated using equation (1) of Bertrand and Gayda in ref. 58 which gives principal g values of $[7g_{1x} - 4g_e + 32\lambda_2\{\sin^2(\theta + \frac{\pi}{3})\}/\Delta_{yz}]/3$, $[7g_{1y} - 4g_e + 32\lambda_2\{\sin^2(\theta - \frac{\pi}{3})\}/\Delta_{xz}]/3$ and $[7g_{1z} - 4g_e + 32\lambda_2\{\sin^2\theta\}/\Delta_{xy}]/3$ as a function of the rhombic distortion mixing parameter θ, with $g_{1x} = 2.015$, $g_{1y} = 2.034$, $g_{1z} = 2.030$, $\lambda_2 = -80$ cm^{-1} and $\Delta_{yz} = 4000$, $\Delta_{xz} = 6000$ cm^{-1} (· · · ·) typical for L = $(SR)_2$; $\Delta_{yz} = 2040$, $\Delta_{xz} = 820$ cm^{-1} (– – – –) typical for L = OS donor; $\Delta_{yz} = 1850$, $\Delta_{xy} = 700$, $\Delta_{xz} = 15\,000$ cm^{-1} (——) typical of Rieske-type proteins. The filled symbols correspond to the g values of Table 5 and represent the co-ordination types NS (◆), NN (■), NO (●); the OS data represented by the smaller triangular symbols are described in the text

The ESR linewidths of $[2Fe–2S]^+$ proteins and inorganic complexes show temperature-dependent broadening indicative of an Orbach relaxation mechanism involving an excited spin-state level.[55,56,26] The well resolved g_1 peak in the spectrum of reduced **1** shows such typical behaviour, approximately doubling in width as the temperature is raised from 100 to 200 K.

As described previously, the tetrabenzimidazolate co-ordinated complexes **4** and **5** are thermally stable at ambient temperatures on reduction. However, as judged by diminution of their ESR signals at 77 K, **1**, **2** and **3** reduced in dmf have ambient-temperature half-lives of approximately 20 h, 1 h and 20 min respectively. These thermal stabilities are rough guides only, being dependent on temperature, and probably also concentration. For example a 1.5 mmol dm^{-3} solution of reduced **2** is found to be stable at −40 °C. The room-temperature stabilities of these $[2Fe–2S]^+$ complexes are greatly augmented by benzimidazolate co-ordination in comparison to thiolate,[21,26] phenolate[31] or carboxylate[32] ligation.

Before assignment of the ESR spectra for the reduction products of complexes **1**–**5**, the somewhat unusual behaviour of $[2Fe–2S]^+$ complexes in frozen aprotic solvents should be briefly reviewed. The $[Fe_2S_2(SR)_4]^{3-}$ ferredoxins and inorganic complexes have ESR spectra characterised by average g values (g_{av}) of *ca.* 1.96. Radically different ESR lineshapes are observed on reduction of $[2Fe–2S]^{2+}$ complexes co-ordinated by monodentate thiolate ligands in solvent mixtures which freeze as glasses.[26] In vitreous *N*-methylpyrrolidinone these have $g_{av} = 1.91$–1.92, whilst in vitreous dmf $g_{av} \approx 1.93$, though the latter type of lineshape transforms to the former on annealing the sample. We have interpreted this behaviour as resulting from a chemical modification of $[Fe_2S_2(SR)_4]^{3-}$ in the glassy solvent state involving substitutional or additional co-ordination possibly by solvent.[26] The $g_{av} = 1.91$–1.92 spectra of this type show a strong correlation with spectra for $[Fe_2S_2(OR)_4]^{3-}$ (R = aryl) and the Rieske-type proteins.[5]

In pure frozen dmf or *N*-methylpyrrolidinone solvents, which crystallise on freezing, the well formed ESR spectra of reduced complexes **1**–**5** show no evidence of sub-spectra due to chemical modification of the type found for monodentate thiolate co-ordination. With the addition of $[NBu^n_4]ClO_4$ to the solvents, such that they freeze as glasses, for tetrabenzimidazolate co-ordination the stable reduced form, **6**, shows only linewidth narrowing due to improved interspin isolation, the principal g values being essentially unchanged. Reduced **1** and **2**, however, show ESR spectral changes in vitreous frozen *N*-methylpyrrolidinone which are indicative of some structural heterogeneity. Spectra of reduced **1** in glassy *N*-methylpyrrolidinone show two sub-spectra of approximately equal magnitude. One corresponds to the signal depicted in Fig. 3, the other has $g_2 = 1.950$ and $g_3 = 1.86$. The latter features are also weakly present in dilute glassy dmf solutions of reduced **1**. In view of the fact that g_{av} for this spectrum is very little different from g_{av} as recorded in Table 5, it seems likely that the species responsible may be a geometric isomer rather than the result of some chemical modification by solvent.

For reduced complex **2** in vitreous *N*-methylpyrrolidinone the ESR spectrum has features at $g = 2.041$, 1.918, 1.71 ($g_{av} = 1.89$) compared to $g = 2.029$, 1.915, 1.76 ($g_{av} = 1.90$) in pure *N*-methylpyrrolidinone. It is difficult to determine whether this small change reflects a ligand modification of the type found for the monodentate thiolate dimers or can be attributed to a stereochemical difference.

We assign the ESR spectra of Figs. 3–5 to the $[Fe_2S_2L_2]^{3-}$ one-electron reduction products. In the case of reduced complexes **4** and **5** this follows plainly from the corroborating spectroscopic and analytical evidence for the isolable compound **6**. For reduced **1** and **2** the conclusion is consistent with interpretation of spectral lineshapes from the wide range of $[2Fe–2S]^+$ complexes we have investigated.[21,26,31–33]

Bertrand and Gayda[57,58] have accounted for the correlation of g-tensor principal components with the separation of the lowest two g values for $[Fe_2S_2(SR)_4]^{3-}$ ferredoxins by using a ligand-field model to relate $(g_2 - g_3)$ to a variable weak rhombic distortion in the ligand environment of the iron(II) ion. Their theoretical best fit for the correlation between the lower two g values and their separation in $[2Fe–2S]^+$ ferredoxins is shown by the upper pair of dotted lines in Fig. 6 originating at $g \approx 1.94$. We found that the g values of synthetic $[Fe_2S_2(SR)_4]^{3-}$ complexes fitted well to these curves.[26]

A similar theoretical analysis employing a set of iron(II) orbital energy levels, which may be interpreted as arising from a large inequivalence between the bridging sulfide and terminal ligands,[5] leads to the set of full-line curves in Fig. 6, which have $g_{av} \approx 1.89$–1.92 and provide a good fit to the ESR g parameters of the Rieske-type proteins. The g values for $[Fe_2S_2(OR)_4]^{3-}$ (R = aryl) and the supposedly solvent ligand-substituted $[Fe_2S_2(SR)_4]^{3-}$ complexes also fit well to these curves.

The remaining pair of dashed lines originating at $g \approx 1.89$ in Fig. 6 are a theoretical fit to the g values found for $[Fe_2S_2L_2]^{3-}$ complexes where L is a mixed-ligand bidentate chelate with oxygen and sulfur donors [though in strict terms the analytical model is for C_{2v} symmetry at the iron(II) ion]. The upward pointing triangles are the g data for $[2Fe–2S]^+$ complexes having the carboxylate–thiolate ligands $O_2CC_6H_4S$-2, $O_2CC_6H_4CH_2S$-2 and $O_2CCH_2C_6H_4S$-2, for both dmf and *N*-methylpyrrolidinone solutions.[32] Data for complexes having 2-$OC_6H_4C_6H_4S$-2 and $OC_6H_4CH_2S$-2 ligands[33] are represented by downward-pointing triangles. We have not previously published plots of these data and do so here for purposes of comparison with complexes **1**–**5**, since the SO co-ordinated $[2Fe–2S]^+$ complexes form a third grouping having fairly well correlated g parameters.

The g values from Table 5 are plotted in Fig. 6. From this an ordering of ligand type can be established for g_2 and g_3 mag-

nitude, independent of the small rhombic distortion within a correlated group: SS > NS > NN > OS > NO ≈ OO. This sequence follows that for the electronegativities (S < N < O) and can in simple terms be related to the degree of inequivalence between bridging and terminal ligands.

Although for reduced complex **5** the g values are rather lower than for reduced **4**, on which previous analysis was based,[15] it is still apparent that benzimidazolate co-ordination alone is insufficient to account for the very low g_2 and g_3 values in the Rieske-type proteins. This can be extended to imidazolate co-ordination on the basis of ESR observations for the partially characterised $[Fe_2S_2L_2]^{3-}$ [H_2L = 2,2-bis-(imidazolyl)propane], which on lineshape simulation has g values of 2.014, 1.924 and 1.841 (g_{av} = 1.926), quite similar to those of reduced **5**.

Reduced complex **2** fits very well into the grouping for the Rieske-type proteins, having g values closely similar to those of benzene dioxygenase from *P. putida* (2.018, 1.917 and 1.754; g_{av} = 1.896).[51]

These results indicate that co-ordination by an oxygen-containing ligand, in addition to the nitrogen co-ordination indicated by electron nuclear double resonance (ENDOR) and electron spin echo envelope modulation (ESEEM), is necessary to bring the lowest g values of the Rieske-type proteins into the observed range. We note that for all the phylogenetically diverse Rieske proteins for which amino-acid sequence information is currently available there is a conserved tyrosine close to cysteine and histidine residues which are regarded as possible ligands to the [2Fe–2S].[59]

However, the most recent exacting ^{15}N ENDOR investigations[7,8] indicate that in the Rieske-type centres of the phthalate dioxygenase from *P. cepacia* and the cytochrome bc_1 complex from *Rhodopseudomonas capsulatus* there are two nitrogen ligands from histidine residues. From the perspective of ESR spectroscopy of inorganic model complexes for Rieske-type proteins, two significant questions require resolution. First the effects on the g tensor of co-ordination by imidazole rather than imidazolate. Presently no [2Fe–2S] complexes having any neutral ligands have been synthesised. Secondly is the effect on the g tensor of changes in co-ordination at the iron(III) ion, which we have assumed to be small. The synthesis of unsymmetrical $(RS)_2FeS_2FeX(Y)$ complexes as more exact models of the proposed co-ordination in Rieske-type proteins would most likely require a semi-rigid planar macrocyclic encapsulation to promote robust [2Fe–2S] attachment and thus circumvent the facile statistical equilibration of the co-ordination due to ligand substitutional lability.

Conclusion

(1) Benzimidazolate ligands readily substitute for chloride in $[Fe_2S_2Cl_4]^{2-}$ to give stable $[Fe_2S_2L_2]^{2-}$ complexes where L is a bidentate chelate.

(2) For the mixed-donor ligands L^1–L^3 the resulting complexes demonstrate geometric co-ordination isomerism in their ^1H NMR spectra.

(3) The ^{57}Fe Mössbauer isomer shift is judged insufficiently sensitive in correlation to ligand type to allow diagnosis of the non-cysteinyl co-ordination in the Rieske-type proteins, but is observed not to discount co-ordination by oxygen.

(4) Benzimidazolate co-ordination is found to cause positive shifts in the first reduction half-wave potential relative to thiolate co-ordination. These shifts are comparable to those for Rieske-type proteins relative to tetracysteinyl ferredoxins.

(5) The concomitant stabilisation of the $[2Fe–2S]^+$ reduced species has allowed isolation of the first such complex, $[NEt_4]_3[Fe_2S_2L^4{}_2]$.

(6) Although in solution this complex is found to undergo rapid intervalence electron transfer on the ^1H NMR time-scale, the faster ^{57}Fe Mössbauer time-scale allows observation of valence trapping as the temperature is lowered.

(7) Analysis of the g tensors of these and other reduced complexes indicates the ordering of the ligand type NS < NN < SO < NO ≈ OO in terms of effectiveness in lowering g_2 and g_3 from their values in $[Fe_2S_2(SR)_4]^{3-}$.

(8) Imidazolate co-ordination alone is deemed insufficient to account for the low g_2 and g_3 values in the Rieske-type proteins. However, these values are matched closely by reduced complex **2** which has nitrogen and oxygen ligands. Attention is drawn to the presence of a conserved tyrosine residue in the ligand region of all Rieske-type protein amino-acid sequences, but also to the need for further model studies employing neutral imidazole ligands and unsymmetrical [2Fe–2S] co-ordination to assist in resolution of the disparity with ENDOR evidence for two histidine imidazole ligands in these proteins.

Acknowledgements

We are grateful to Chris Lawrence and Dr. B. W. Fitzsimmons of Birkbeck College for measuring and fitting the Mössbauer spectra.

References

1 R. H. Holm and J. A. Ibers, *Iron–Sulfur Proteins*, ed. W. Lovenberg, Academic, New York, 1977, vol. 3, ch. 7.
2 J. M. Berg and R. H. Holm, *Iron–Sulfur Proteins*, ed. T. G. Spiro, Wiley, New York, 1982, ch. 1.
3 J. A. Fee, D. Kuila, M. W. Mather and T. Yoshida, *Biochim. Biophys. Acta*, 1986, **853**, 153.
4 J. A. Fee, K. L. Findling, T. Yoshida, R. Hille, G. E. Tarr, D. O. Hearshen, W. R. Dunham, E. P. Day, T. A. Kent and E. Münck, *J. Biol. Chem.*, 1984, **259**, 124.
5 P. Bertrand, B. Guigliarelli, J. P. Gayda, P. Beardwood and J. F. Gibson, *Biochim. Biophys. Acta*, 1985, **831**, 261.
6 J. S. Rieske, R. E. Hansen and W. S. Zaugg, *J. Biol. Chem.*, 1964, **239**, 3017.
7 R. J. Gurbiel, C. J. Batie, M. Sivaraja, A. E. True, J. A. Fee, B. M. Hoffman and D. P. Ballou, *Biochemistry*, 1989, **28**, 4861.
8 R. J. Gurbiel, T. Ohnishi, D. E. Robertson, F. Daldal and B. M. Hoffman, *Biochemistry*, 1991, **30**, 11579.
9 R. D. Britt, K. Sauer, M. P. Klein, D. B. Knaff, A. Kriauciunas, C.-A. Yu, L. Yu and R. Malkin, *Biochemistry*, 1991, **30**, 1892.
10 H.-T. Tsang, C. J. Batie, D. P. Ballou and J. E. Penner-Hahn, *Biochemistry*, 1989, **28**, 7233.
11 L. Powers, H. Schägger, G. von Jagow, J. Smith, B. Chance and T. Ohnishi, *Biochim. Biophys. Acta*, 1989, **975**, 293.
12 D. Kuila, J. A. Fee, J. R. Schoonover, W. H. Woodruff, C. J. Batie and D. P. Ballou, *J. Am. Chem. Soc.*, 1987, **109**, 1559.
13 L. A. Graham and B. L. Trumpower, *J. Biol. Chem.*, 1991, **266**, 22485.
14 D. L. Gatti, S. W. Meinhardt, T. Ohnishi and A. Tzagoloff, *J. Mol. Biol.*, 1989, **205**, 421.
15 P. Beardwood and J. F. Gibson, *J. Chem. Soc., Chem. Commun.*, 1986, 490.
16 D. W. Hein, R. J. Alheim and J. J. Leavitt, *J. Am. Chem. Soc.*, 1957, **79**, 427.
17 J. Sluka, J. Novak and Z. Budesinsky, *Collect. Czech. Chem. Commun.*, 1976, **41**, 3628.
18 P. C. Vyas, C. K. Oza and A. K. Goyal, *Chem. Ind. (London)*, 1980, 287.
19 J. J. Bloomfield, *J. Org. Chem.*, 1961, **26**, 4112.
20 Y. Do, E. D. Simhon and R. H. Holm, *Inorg. Chem.*, 1983, **22**, 3809.
21 P. Beardwood, J. F. Gibson, C. E. Johnson and J. D. Rush, *J. Chem. Soc., Dalton Trans.*, 1982, 2015.
22 L. K. White and R. L. Belford, *J. Am. Chem. Soc.*, 1976, **98**, 4428.
23 P. Beardwood, Ph.D. Thesis, University of London, 1983.
24 J. J. Mayerle, S. E. Denmark, B. V. DePamphilis, J. A. Ibers and R. H. Holm, *J. Am. Chem. Soc.*, 1975, **97**, 1032.
25 G. B. Wong, M. A. Bobrik and R. H. Holm, *Inorg. Chem.*, 1978, **17**, 578.
26 P. Beardwood and J. F. Gibson, *J. Chem. Soc., Dalton Trans.*, 1983, 737.
27 D. Coucouvanis, D. Swenson, P. Stremple and N. C. Baenziger, *J. Am. Chem. Soc.*, 1979, **101**, 3392.
28 H. Strasdeit, B. Krebs and G. Henkel, *Inorg. Chim. Acta*, 1984, **89**, L11.
29 A. Salifoglou, A. Simopoulos, A. Kostikas, R. W. Dunham, M. G. Kanatzidis and D. Coucouvanis, *Inorg. Chem.*, 1988, **27**, 3394.
30 W. E. Cleland and B. A. Averill, *Inorg. Chem.*, 1984, **23**, 4192.

31 P. Beardwood and J. F. Gibson, *J. Chem. Soc., Chem. Commun.*, 1985, 102.
32 P. Beardwood and J. F. Gibson, *J. Chem. Soc., Chem. Commun.*, 1985, 1345.
33 P. Beardwood and J. F. Gibson, *Polyhedron*, 1988, **7**, 1911.
34 G. Guillot, E. Mulliez, P. Luduc and J.-C. Chottard, *Inorg. Chem.*, 1990, **29**, 577.
35 J. Cambray, R. W. Lane, A. G. Wedd, R. W. Johnson and R. H. Holm, *Inorg. Chem.*, 1977, **16**, 2565.
36 P. Beardwood and J. F. Gibson, *J. Chem. Soc., Dalton Trans.*, 1984, 1507.
37 J. G. Reynolds and R. H. Holm, *Inorg. Chem.*, 1980, **19**, 3257.
38 R. H. Holm, W. D. Phillips, B. A. Averill, J. J. Mayerle and T. Herskovitz, *J. Am. Chem. Soc.*, 1974, **96**, 2109.
39 J. G. Reynolds, E. J. Laskowski and R. H. Holm, *J. Am. Chem. Soc.*, 1978, **100**, 5315.
40 L. B. Dugad, G. N. LaMar, L. Banci and I. Bertini, *Biochemistry*, 1990, **29**, 2263.
41 I. Bertini, G. Lanini and C. Luchinat, *Inorg. Chem.*, 1984, **23**, 2729.
42 L. Skjeldal, J. L. Markley, V. M. Coghlan and L. E. Vickery, *Biochemistry*, 1991, **30**, 9078.
43 D. Kuila and J. A. Fee, *J. Biol. Chem.*, 1986, **261**, 2768.
44 P. J. Geary and D. P. E. Dickson, *Biochem. J.*, 1981, **195**, 199.
45 W. R. Dunham, A. J. Bearden, I. T. Salmeen, G. Palmer, R. H. Sands, W. H. Orme-Johnson and H. Beinert, *Biochim. Biophys. Acta*, 1971, **253**, 134.
46 R. E. Anderson, W. R. Dunham, R. H. Sands, A. J. Bearden and H. L. Crespi, *Biochim. Biophys. Acta*, 1975, **408**, 306.
47 E. Münck, P. E. Debrunner, J. C. M. Tsibris and I. C. Gunsalus, *Biochemistry*, 1972, **11**, 855.
48 R. Cammack, K. K. Rao, D. O. Hall and C. E. Johnson, *Biochem. J.*, 1971, **125**, 849.
49 K. K. Rao, R. Cammack, D. O. Hall and C. E. Johnson, *Biochem. J.*, 1971, **122**, 257.
50 P. Bertrand and J.-P. Gayda, *Biochim. Biophys. Acta*, 1982, **680**, 331.
51 P. J. Geary, F. Saboowalla, D. Patil and R. Cammack, *Biochem. J.*, 1984, **217**, 667.
52 R. C. Prince, J. G. Lindsay and P. L. Dutton, *FEBS Lett.*, 1975, **51**, 108.
53 W. D. Bonner and R. J. Prince, *FEBS Lett.*, 1984, **177**, 47.
54 R. J. Kassner and W. Yang, *J. Am. Chem. Soc.*, 1977, **99**, 4351.
55 J. P. Gayda, J. F. Gibson, R. Cammack, D. O. Hall and R. Mullinger, *Biochim. Biophys. Acta*, 1976, **434**, 154.
56 P. Beardwood, J. F. Gibson, P. Bertrand and J. P. Gayda, *Biochim. Biophys. Acta*, 1983, **742**, 426.
57 P. Bertrand and J. P. Gayda, *Biochim. Biophys. Acta*, 1979, **579**, 107.
58 P. Bertrand and J. P. Gayda, *Biochim. Biophys. Acta*, 1980, **625**, 337.
59 M. Nishikimi, Y. Hosokawa, H. Toda, H. Suzuki and T. Ozawa, *Biochem. Int.*, 1990, **20**, 155; M. Nishikimi, Y. Hosokawa, H. Toda, H. Suzuki and T. Ozawa, *Biochem. Biophys. Res. Commun.*, 1989, **159**, 19; J. Steppuhn, C. Rother, J. Hermans, T. Jansen, J. Salnikow, G. Hauska and R. G. Herrmann, *Mol. Gen. Genet.*, 1987, **210**, 171; H. Schägger, U. Borchart, W. Machleidt, T. A. Link and G. Von Jagow, *FEBS Lett.*, 1987, **219**, 161; S. Usui, L. Yu and C.-A. Yu, *Biochem. Biophys. Res. Commun.*, 1990, **167**, 575; U. Harnish, H. Weiss and W. Sebald, *Eur. J. Biochem.*, 1985, **149**, 95; J. O. Beckmann, P. O. Ljungdahl, J. L. Lopez and B. L. Trumpower, *J. Biol. Chem.*, 1987, **262**, 8901; E. Davidson and F. Daldal, *J. Mol. Biol.*, 1987, **195**, 13; G. Hauska, W. Nitschke and R. G. Herrmann, *J. Bioenerg. Biomem.*, 1988, **20**, 211; C.-H. Yun, R. Beci, A. R. Crofts, S. Kaplan and R. B. Gennis, *Eur. J. Biochem.*, 1990, **194**, 399; T. Kallas, S. Spiller and R. Malkin, *Proc. Natl. Acad. Sci. USA*, 1988, **85**, 5794; C. Majewski and A. Trebst, *Mol. Gen. Genet.*, 1990, **224**, 373; L. Thöny-Meyer, D. Stax and H. Hennecke, *Cell*, 1989, **57**, 683; J. Verbist, F. Lang, N. Gabellini and D. Oesterhelt, *Mol. Gen. Genet.*, 1989, **219**, 445; B. Kurowski and B. Ludwig, *J. Biol. Chem.*, 1987, **262**, 13805.

Received 7th February 1992; *Paper* 2/00673A